Steel and Composite Structures, *Vol. 30, No. 4 (2019) 351-364*
DOI: https://doi.org/10.12989/scs.2019.30.4.351

Experimental study on cyclically-damaged steel-concrete composite joints subjected to fire

Zhongnan Ye [1], Shouchao Jiang [1], Amin Heidarpour [*2], Yingchao Li [1] and Guoqiang Li [1]

[1] *College of Civil Engineering, Tongji University, Shanghai, 200092, China*
[2] *Department of Civil Engineering, Monash University, VIC 3800, Melbourne, Australia*

(*Received December 30, 2017, Revised November 8, 2018, Accepted February 20, 2019*)

Abstract. Earthquake and fire are both severe disasters for building structures. Since earthquake-induced damage will weaken the structure and reduce its fire endurance, it is important to investigate the behavior of structure subjected to post-earthquake fire. In this paper, steel-concrete composite beam-to-column joints were tested under fire with pre-damage caused by cyclic loads. Beforehand, three control specimens with no pre-damage were tested to capture the static, cyclic and fire-resistant performance of intact joints. Experimental data including strain, deflection and temperature recorded at several points are presented and analyzed to quantify the influence of cyclic damage on fire resistance. It is indicated that the fire endurance of damaged joints decreased with the increase of damage level, mainly due to faster heating-up rate after cyclic damage. However, cracks induced by cyclic loading in concrete are found to mitigate the concrete spalling at elevated temperatures. Moreover, the relationship between fire resistance and damage degree is revealed from experimental results, which can be applied in fire safety design and is worthwhile for further research.

Keywords: post-earthquake fire; composite joint; cyclic loading; fire-resistant performance; fire endurance

1. Introduction

When building safety is concerned, it is of great importance to investigate the fundamental behavior of structures subjected to fire after earthquake in seismic prone regions (Kato *et al*. 1980). Generally, the possibility of a fire disaster is much higher when earthquake occurs. In addition, losses caused by post-earthquake fires could be more severe compared to those resulting directly from the shaking. In accordance with current design methods and standards, most structures are designed allowing some extent of deformation during strong earthquakes, which means reduction of fire resistance caused by earthquake-induced damage (Tremblay *et al*. 1996). Therefore, it is rational that structures with pre-damage deformation might be more vulnerable when exposed to fires (Mirmomeni *et al*. 2017, Azhari *et al*. 2018).

Steel-concrete composite structures and members are extensively used in critical infrastructure, since they combine both steel and concrete material advantages to establish a practical structural system. Since 1980s, the focus was gradually changed from individual composite members (i.e., beams (Valente and Cruz 2010) and columns (Sevim 2017)) to composite frames and connections (Ma *et al*. 2011). For instance, Liew *et al*. (2004) conducted several tests on steel-concrete composite beam-to-column joints subjected to reversal loading, from which the moment-rotation relationships for the joints were obtained to reveal a good energy dissipation performance of the joints. Pecce and Rossi (2015) investigated the experimental behavior of joints in composite moment resisting frames, describing the performance of the joints in terms of resistance, ductility, dissipative energy and stiffness deterioration. Amadio *et al*. (2017) implemented numerical analysis on steel-concrete composite welded joints to simulate both global and local behavior subjected to seismic loads. Moreover, some new types of composite joints have also been proposed, such as tubular T-joints reinforced with grouted sleeve (Jiang *et al*. 2017) and pre-tightened teeth composite tubular connection (Li *et al*. 2017), taking advantages of steel and steel-concrete composite material. Even now, the performance of steel-concrete composite beam-to-column joints is still a significant problem deserving in-depth exploration (Zhu *et al*. 2017, Xiao *et al*. 2017).

With the development of economy and technology, more comprehensive considerations are needed for structural design and construction under multi-phase loading scenarios such as post-earthquake fire since the performance of structures is profoundly different from when the structures is exposed to either earthquake (Dubina *et al*. 2002) or fire (Santiago *et al*. 2008). For instance, Sinaie *et al*. (2014) investigated mechanical properties of structural mild steel under elevated temperatures after cyclical damage and proposed a stress-strain-temperature model for mild steel, implying that the history of cyclic loading should be considered in the post-earthquake fire-resistant design. Song *et al*. (2017) conducted a series of experiments on post-earthquake fire performance of steel beam-to-column connections, in which the load-carrying capacity was found to decreasing significantly with the

*Corresponding author, Ph.D.,
E-mail: amin.heidarpour@monash.edu

ISSN: 1229-9367 (Print), 1598-6233 (Online)

increase of pre-damage level. For composite structures, a series of experimental research on concrete-filled tubular beam-to column joints have been performed (Alderighi *et al*. 2008, Pucinotti *et al*. 2011a, b), which aimed to develop a performance-based multi-objective design method. They noticed the necessity of taking into account the pre-damage in fire resistance analysis. However, in their research works, the pre-damaged specimens were loaded monotonically to "imitate" the cyclic damage before fire test, which is not the real case for the "post-earthquake" scenario.

Although it is indicated from previous research works that cyclic-induced damage may or may not influence the fire resistance of a structure, it is time to take a further step into the question how fire resistance performance varies with the level of seismic-induced damage. However, due to the lack of adequate experimental data, the quantitative influence of cyclic-induced damage on fire resistance performance remains unclear. It is necessary to conduct pertinent experimental research to provide essential quantitative data as the foundation for further research to propose a robust model.

Therefore, this paper deals with a series of experimental tests to explore the behavior of cyclically-damaged steel-concrete composite connections at elevated temperatures. The experimental data presented in this paper are of practical value for further understanding of the performance and behavior of steel-concrete composite beam-to-column joints subjected to post-earthquake fire.

2. Experimental program

To investigate the fundamental performance of steel-concrete composite joints subjected to fire after cyclic loading, five specimens (named from SP1 to SP5) shown in Table 1 were designed and tested. SP1, SP2 and SP3 are control specimens with no pre-damage while SP4 and SP5 are cyclically damaged specimens tested under fire. Such a testing arrangement allows to thoroughly investigate the deformation characteristics, mechanical responses and failure modes of both intact and pre-damaged specimens at room and elevated temperatures.

2.1 Specimens and materials

As depicted in Fig. 1, the 5 specimens are of the same size (5630 mm × 982 mm × 900 mm) where each one consists of one welded H-section steel column (240 mm × 240 mm × 12 mm × 14 mm), two welded H-section steel beams (300 mm × 150 mm × 8 mm × 12 mm), and one

Table 1 Experimental program

No.	Description
SP1	Monotonic test on intact joint at room temperature
SP2	Cyclic test on intact joint at room temperature
SP3	Fire test on intact joint
SP4	Fire test on partially damaged joint (low damage level)
SP5	Fire test on partially damaged joint (high damage level)

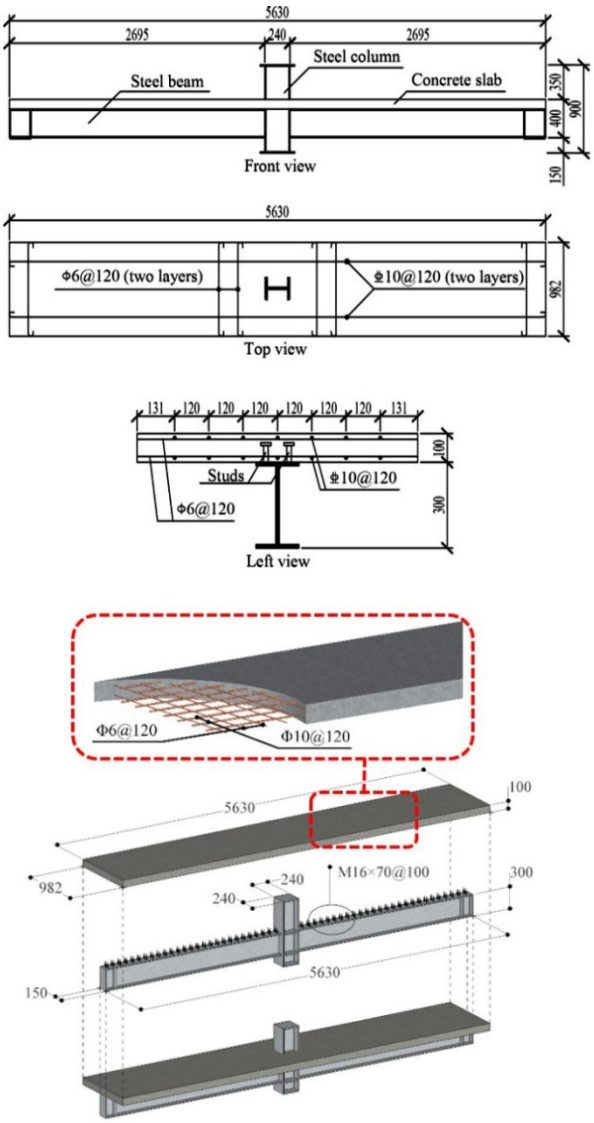

Fig. 1 Configuration of specimens

reinforced concrete (RC) flat slab (5630 mm × 982 mm × 100 mm). The RC slab was connected to the upper flange of steel beams with studs. Two rows of cheese head studs with diameter of 16 mm were manually welded to the upper flange of steel beams to ensure the full shear connection between the RC slab and the steel beams. The specification of specimens is presented in Table 2.

Table 2 Specification of specimens (dimensions in mm)

No.	Member	Grade	Cross-section	Length
1	Steel beam	S355JR	H300×150×8×12	2695
2	Steel column	S355JR	H240×240×12×14	900
3	Concrete slab	C30	100×982	5630
4	Transverse reinforcement	HPB300	Φ6@120	-
5	Longitudinal reinforcement	HPB400	Φ10@120	-
6	Shear studs for arc stud welding	ML15	M16×70@100mm	-

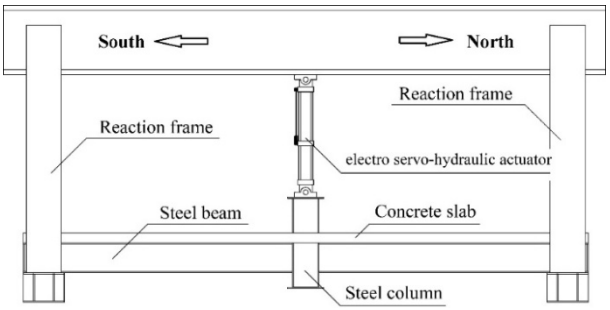

Fig. 2 Test device for monotonic, cyclic and pre-damage cyclic test

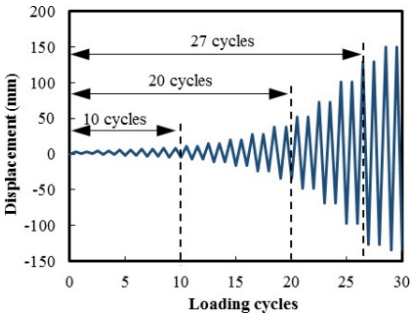

Fig. 3 Loading process for SP2, SP4 and SP5 specimens

Table 3 Material properties

No.	Material	Member	Property	Actual value (MPa)
1	S355JR (8 mm)	1	Elasticity modulus	2.1×10^5
			Yield strength	350
			Ultimate strength	495
2	S355JR (12 mm)	1&2	Elasticity modulus	2.1×10^5
			Yield strength	323
			Ultimate strength	505
3	S355JR (14 mm)	2	Elasticity modulus	2.1×10^5
			Yield strength	309
			Ultimate strength	496
4	Concrete (C30)	3	Elasticity modulus	3.0×10^4
			Cube crushing strength	36.6
			Prism crushing strength	27.8
5	HPB300 (6 mm)	4	Elasticity modulus	2.0×10^5
			Yield strength	566
			Ultimate strength	609
6	HPB400 (10 mm)	5	Elasticity modulus	2.1×10^5
			Yield strength	532
			Ultimate strength	549
7	Shear studs (ML15)	6	Elasticity modulus	2.1×10^5
			Yield strength	462
			Ultimate strength	535

Mechanical properties of materials used in the specimens have been obtained from the standard material characteristic tests and are summarized in Table 3. The strength of each material was measured from 3 independent material specimens and the average strength was presented in the table. Specifically, all concrete members were cured for 28 days before material, monotonic, cyclic and fire tests.

2.3 Test Setup and loading protocols

Monotonic test (SP1), cyclic test (SP2), and pre-damage phase of SP4 & SP5 tests were all performed with the test device presented in Fig. 2. After the installation of each specimen, trial load was applied to check all equipment. For the monotonic test (SP1), every 24 kN of load was applied as a unit till 80% of the estimated load bearing capacity was reached. Afterwards, every 12 kN of load was applied as a unit until failure. The monotonic load was applied upward, which means the top surface of the concrete near the joint area was in tension in accordance with the real working conditions. For the cyclic tests (SP2, SP4 and SP5), cyclic loading was applied according to FEMA- 461 (2007) loading protocol as shown in Fig. 3. Note that for SP4 and SP5 specimens it is important to determine the damage degree and corresponding loading cycles. In this research, the damage index model proposed by Niu and Ren (1996) is adopted to evaluate the damage degree of damaged specimens. According to their model, the damage index is obtained from displacement and energy dissipation of the specimen. The damage index D is calculated according to Eq. (1), S_u and E_u are the ultimate displacement and ultimate energy dissipation in monotonic test, $S_{i,\max}$ is the maximum displacement until cycle i, E_i is the energy dissipation in cycle i, α and β are damage parameters related to structural system, respectively. For steel-concrete composite structures, it is suggested that α = 0.1387, β = 0.0814.

$$D=\frac{S_{i,\max}}{S_u}+\alpha\left(\frac{\sum_{i=1}^{n}E_i}{E_u}\right)^{\beta} \quad (1)$$

According to monotonic test, for our specimens, S_u = 157 mm, E_u = 39874 kN·mm. The development trend of

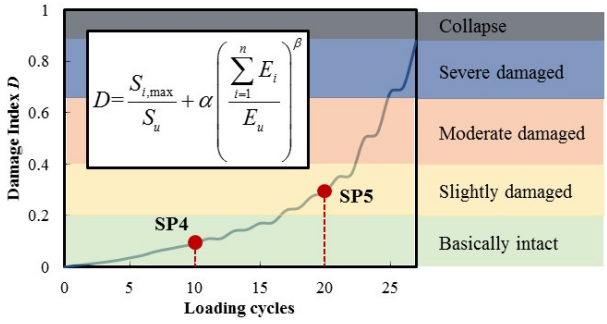

Fig. 4 Damage index of SP2 according to the damage model proposed by Niu and Ren (1996)

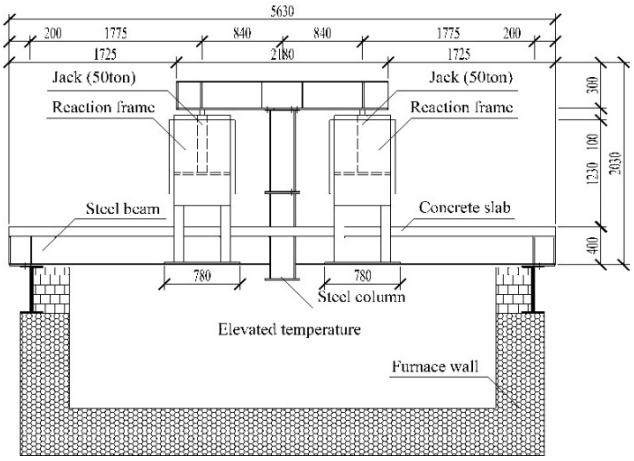

Fig. 5 Test device for fire test

Table 4 Properties of the ceramic fiber blanket

Melting point (°C)	Density (kg/m^3)	Heat conductivity coefficient (W/(m·K))		
		400°C	600°C	800°C
1760	128	0.13	0.19	0.25

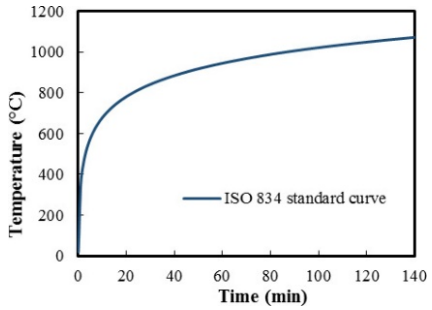

Fig. 6 ISO834 standard curve

damage index for SP2 was plotted in Fig. 4. To perform minor and major pre-damage to SP4 and SP5, 10 load cycles and 20 load cycles were applied respectively (corresponding damage indexes were 0.16 and 0.32, respectively).

All the fire tests (i.e., SP3 and the second phase of SP4 and SP5 tests) were conducted inside the furnace at Tongji University, China as depicted in Fig. 5. The specimen was heated from the bottom side, which means the upper side of the concrete slab was unexposed to fire. Before heating, ceramic fiber blankets as fire protection with low heat conductivity coefficient were covered on all steel members exposed to fire. The properties of the blankets are summarized in Table 4. Constant upward load of 152 kN which is approximately equal to 50% of the ultimate static load bearing capacity of the joint, was applied to the specimen with two jacks before heating. After that, fire test started in which the temperature-time curve followed the standard ISO834 as plotted in Fig. 6 until the specimen failed to carry the applied constant load of 152 kN.

2.3 Measuring points arrangement

During the experiments, relevant quantitative data, including load, displacement, strain, and temperature were measured and recorded. The loads were measured by load cells connected to loading jacks. All displacement data were collected by displacement gages. The arrangement of displacement gages is depicted in Fig. 7(a), where D4 and D5 were installed to measure the deflection at the mid-span of the specimen. Moreover, D11-D14 were designed just for SP1 and SP3 to calculate the rotation of the beam. For the room temperature tests, including monotonic test (SP1), cyclic test (SP2), and pre-damage cyclic tests (SP4 and SP5), 10 strain gages were installed on each specimen as shown in Fig. 7(b) to capture the mechanical response in the joint area. For the fire tests, 15 thermocouples for each specimen were installed at three cross sections (I, II and III) as depicted in Fig. 7(c).

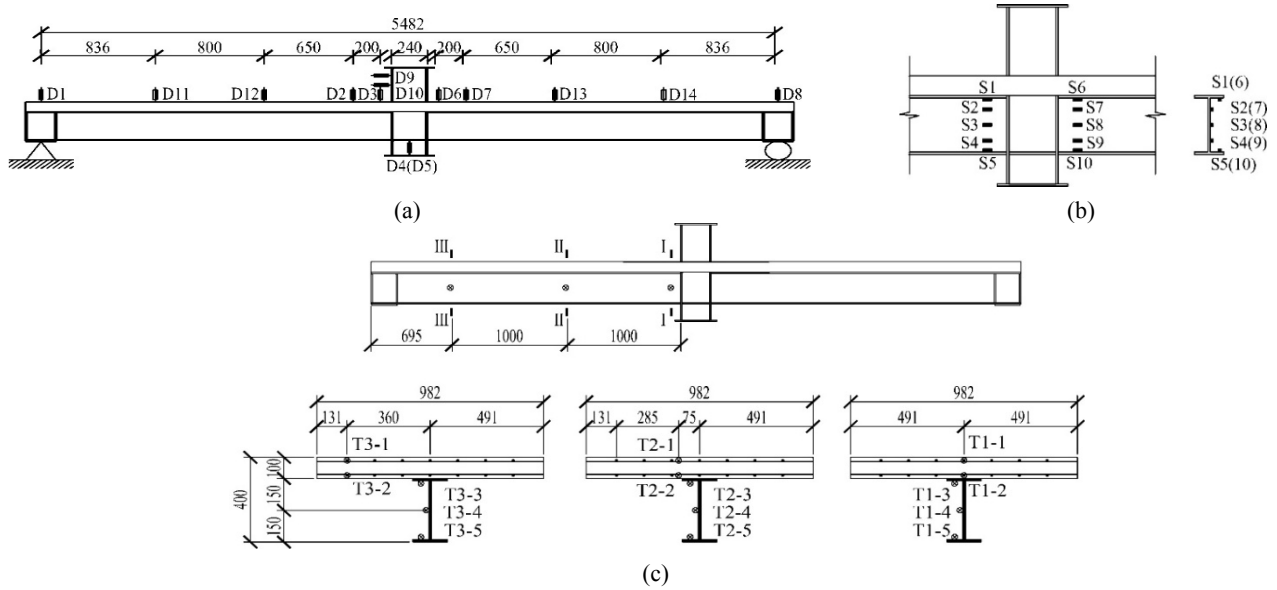

Fig. 7 Arrangement of measuring points for SP3, SP4 and SP5 specimens: (a) displacement gages; (b) strain gages; (c) thermocouples

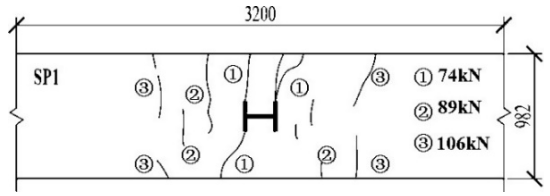

(a) SP1

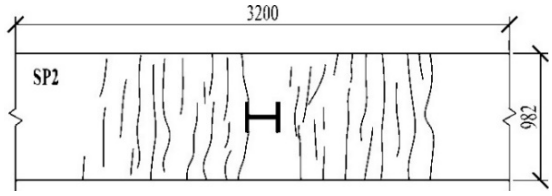

(b) SP2

Fig. 8 Cracks of specimens

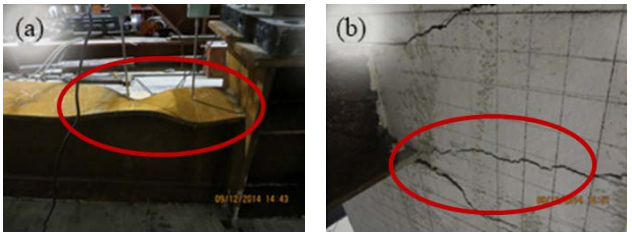

(a) Buckling (b) Cracks near the steel column

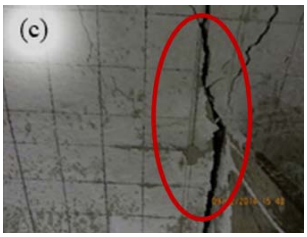

(c) Throughcrack

Fig. 9 Failure mode of SP1 specimen

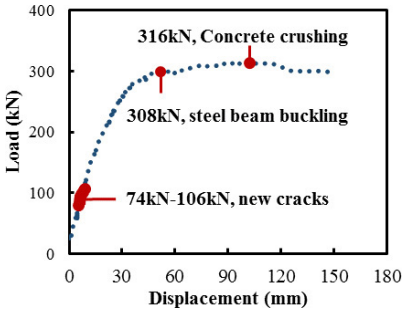

(a) Critical events

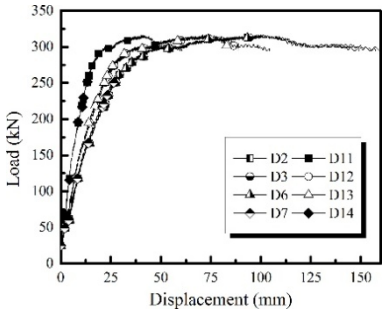

(b) Load vs. displacement

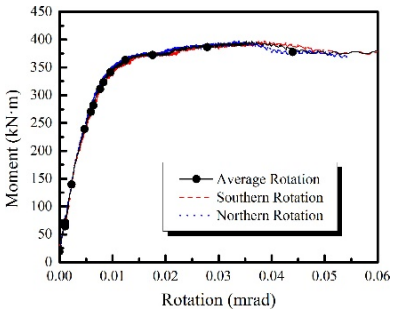

(c) Moment vs. rotation

Fig. 10 Results of SP1 specimen

3. Experimental results

The experimental results including load bearing capacity, failure modes, and deformation of specimens are presented and discussed in this section.

3.1 Monotonic and cyclic tests at room temperature (SP1 and SP2)

The cracks pattern for the monotonic test (SP1) is shown in Fig. 8 where the magnitude of load at onset of each crack has been recorded. The first crack occurred at the mid-span of the specimen where the moment is the largest. In addition, there was no new cracks after the load reached 106 kN, but the existing cracks did develop

Table 5 Experimental phenomena for SP2 specimen

No.	A_i	n	Amplitude of A_i	P (kN)	u (mm)	Comments
1	1-3	1-5	3.41	77	6	Many new cracks (Fig. 11-a)
2	13	25	83.75	309	83	Concrete crumbling at the mid-span (Fig. 11-b) buckling of steel beam lower flange (Fig. 11-c)
3	13	26	83.75	264	83	Buckling of web of steel beam (Fig. 11-d) reinforcement appearing (Fig. 11-e)
4	14	27	128.38	234	125	Large crack through the slab (Fig. 11-f) concrete crushing at the mid-span (Fig. 11-g)

* A_i: the loading grade for cyclic test (each grade was loaded twice); n: serial number of loading cycle, P: the magnitude of hogging load; u: the maximum deflection at the mid span.

continually. When the load reached the value of 308 kN, the lower flange of the steel beam buckled (Fig. 9(a)) and the vertical deformation increased rapidly. At the same time, the cracks went through the whole reinforced concrete near the flanges of steel column (Figs. 9(b) and (c)). After the load reached the value of 316kN, the load decreased slightly with slow increase of the deflection which indicated the joint failure.

To illustrate the mechanical properties of the joint, the deformation at the mid-span of SP1 is plotted in Fig. 10(a), where critical events observed during the experiment are also cited. Besides, according to data from other displacement gages arranged on steel beams, as shown in Fig. 10(b), the rotation at each side was calculated in Fig. 10(c). It is found that plastic deformation developed well in the joint so that the ultimate moment capacity of the joint was 387 kN·m, with the rotation of 30 mrad.

For the cyclic test (SP2), cracks at the upper surface of concrete slab were observed at the end of the first cycle of loading, indicating that the cracking load was smaller than the maximum load of the first cycle (54 kN). As shown in Fig. 11, numerous cracks developed in SP2 due to cyclic loading, which are far more than that in SP1. The events observed of SP2 are summarized in Table 5, with corresponding photos shown in Fig. 11. As shown in Table 5, the ultimate load was 309 kN which occurred at the 25th cycle (upward force) with the displacement of 83 mm at the column. After the 27th cycle where the maximum load and displacement were 234 kN and 126 mm, respectively, the specimen failed due to concrete crushing.

Fig. 12(a) shows the hysteretic curve and skeleton curve at the mid-span of SP2. Unsymmetrically, the maximum upward force is 309 kN and corresponding displacement is 83 mm while the maximum downward force and corresponding average displacement were 437 kN and 114 mm, respectively. It is also indicated that the energy-dissipating capacity of the joint is great, since the hysteretic curve is plump and without pinch phenomenon. According to local skeleton curve of SP2 (Fig. 12(b)), the stiffness started to reduce at 55 kN, followed by a noticeable reduction at 80 kN. This reduction was due to concrete cracking in tension under hogging load when the load exceeded the cracking load. However, when concrete is in compression under sagging load, the slope of the skeleton

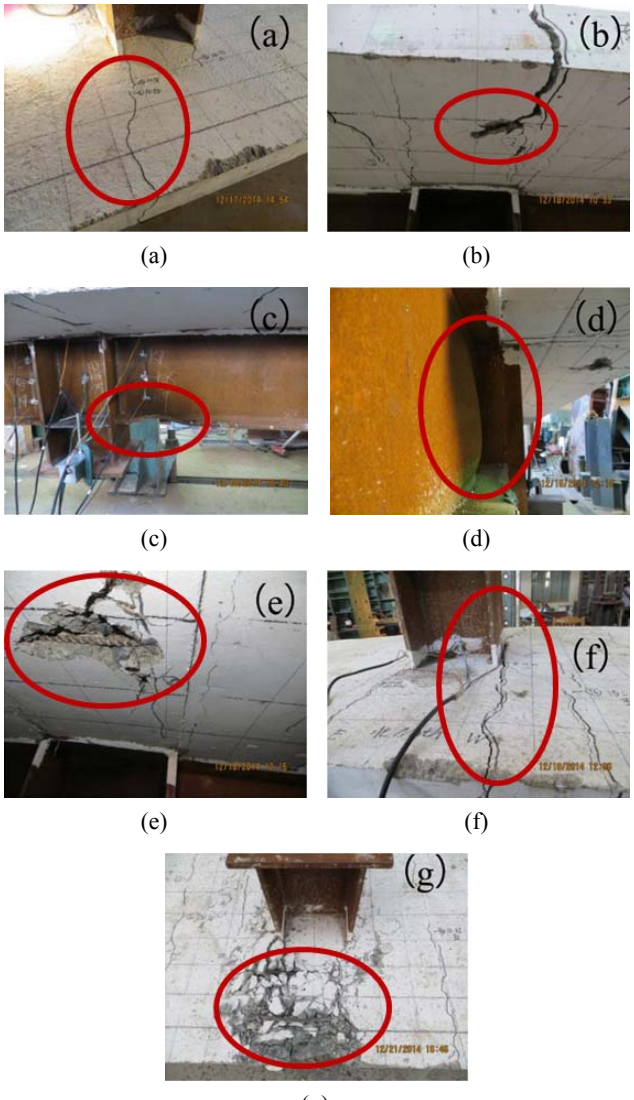

Fig. 11 Phenomena observed in SP2 specimen

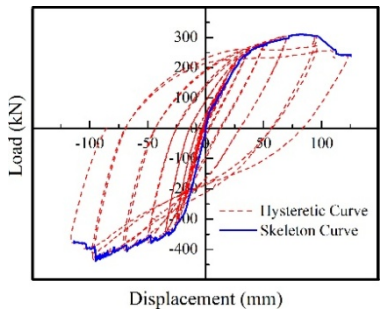

(a) Hysteretic and skeleton curves

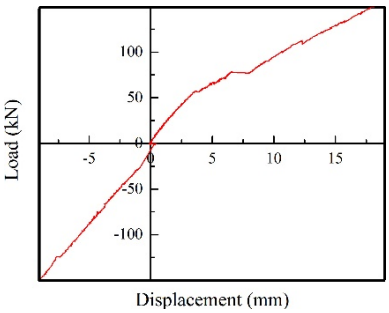

(b) Local skeleton curve

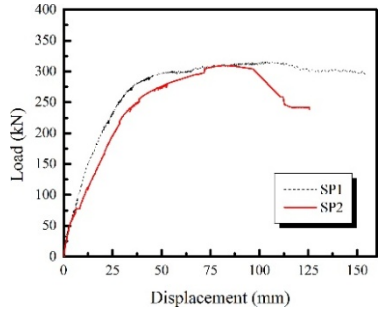

(c) Results of SP1 and SP2

Fig. 12 Results of SP2 specimen (load vs. displacement)

Table 6 Load bearing capacity of SP1 and SP2 specimens

No.	P_u (kN)	u_u (mm)	M_u (kN·m)	θ_u (mrad)
SP1	316	104	397	30
SP2	309	83	387	22

curve remains basically unchanged which means the cracks would close and continue to bear the load without any influence on the joint stiffness.

Comparing the skeleton curve of SP2 with load - displacement curve of SP1 (Fig. 12(c)), it is indicated that the stiffness and load bearing capacity of SP2 are smaller than those of SP1. Besides, the maximum upward force Pu applied by the electro-servo hydraulic actuator and corresponding displacement at the mid-span uu, the maximum moment Mu caused by Pu and corresponding rotation θu of both SP1 and SP2 are presented in Table 6. As shown, the slight reduction in load bearing capacity of SP2 could be attributed to the damage caused by cyclic loading. This is because of numerous cracks in concrete and residual deformation in steel members after reversal loading, which would deteriorate the performance of the specimen.

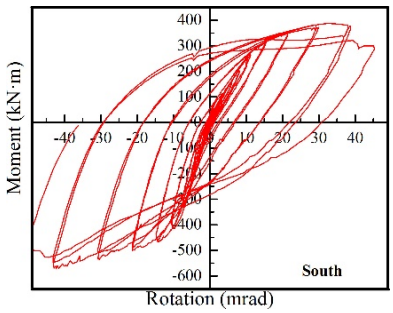

(a) South

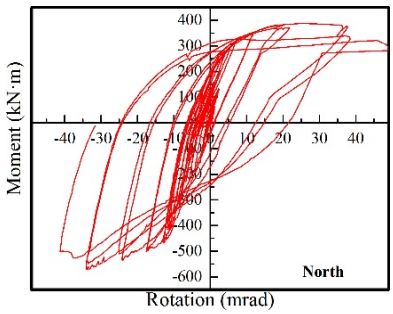

(b) North

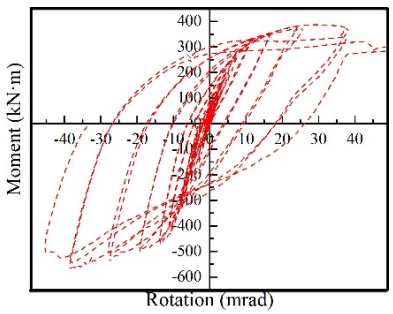

(c) Average

Fig. 13 Results of SP2 specimen (moment vs. rotation)

Similar to SP1, moment-rotation curve for SP2 could be obtained from the displacement gages on the beams. The southern rotation, the northern rotation and their average value are plotted in Fig. 13. It is seen that the ultimate positive moment is 387 kN·m, with the rotation of 30 mrad, and the ultimate negative moment is 577 kN·m, with the rotation of 39 mrad. In the final cycle (27th), the positive moment is 297 kN·m, with the rotation of 52 mrad, and the negative moment is 462 kN·m, with the rotation of 46 mrad. Due to the difference between tensile and compressive capacities of concrete, the moment-rotation hysteretic curves are not symmetric in which higher load bearing capacity is observed in the fourth quadrant of the curve due to the contribution of concrete slab.

3.2 pre-damage cyclic tests (SP4 and SP5)

Pre-damage cyclic tests were conducted to make partial damage on SP4 and SP5 specimens. Fig. 14 depicts the cracks pattern after cyclic loading in the concrete slab of SP4 and SP5, showing that SP5 undertook more cracks due to more cycles and larger amplitude than those applied on SP4. Table 7 compares the values of the mechanical properties of SP4 and SP5 with those obtained for SP2 in the previous section. As shown, the maximum loads applied on SP4 and SP5 are 31% and 77% of SP2 and the values of corresponding displacements are 11% and 37% of SP2, respectively. It is indicated that SP4 has experienced only minor damage as almost no significant plastic deformation has developed during cyclic loading.

In addition, the hysteresis curves of all three tests (SP2, SP4 and SP5) are depicted and compared in Fig. 15. It is seen that the hysteretic curve of SP4 is almost linear and the area of hysteresis curve encircles is quite small, which means ignorable deterioration of stiffness and residual deformation. However, in SP5, the hysteresis curve tends to be "S" type and stiffness of the final cycle is clearly smaller than that of the first cycle. This could be attributed to the cracks developed in concrete and also the yielding of the steel beam. Nevertheless, the envelop area of the load-displacement curve implies that the energy dissipation is much less than that of SP2. From Fig. 15(c), it is found that the hysteresis curve of SP4 is almost the first part of SP5

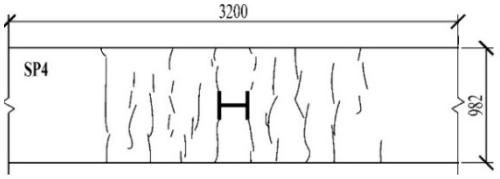

(a) SP4

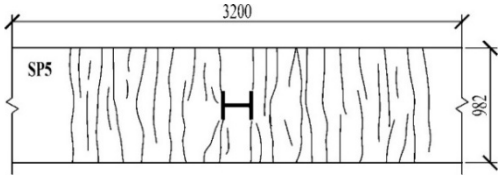

(b) SP5

Fig. 14 Cracks of specimens

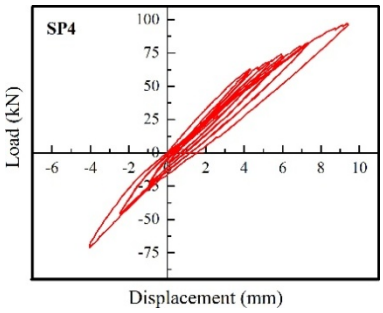

(a) SP4

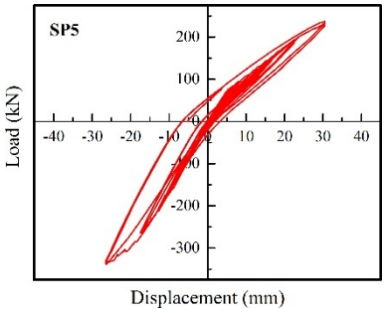

(b) SP5

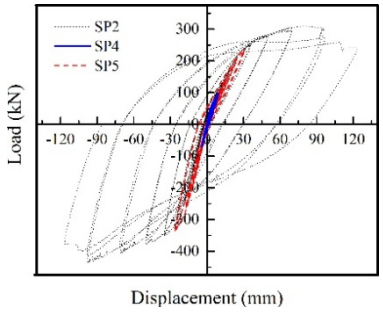

(c) SP2, SP4 and SP5

Fig. 15 Hysteretic curves of specimens

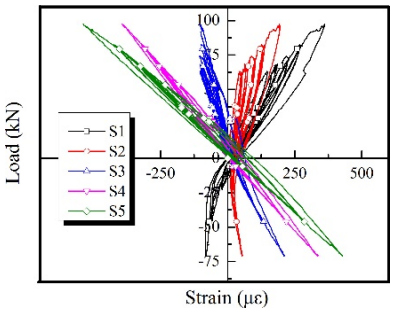

(a) SP4

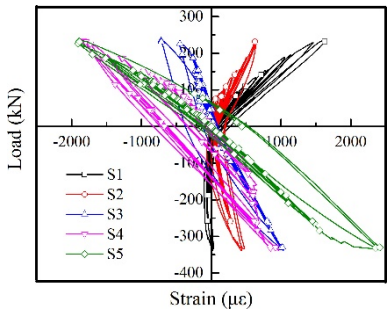

(b) SP5

Fig. 16 Load-strain curves under cyclic loading

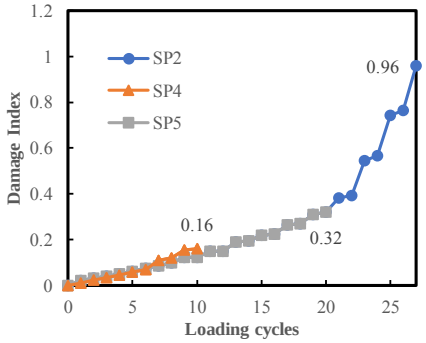

Fig. 17 Damage index results according to the damage model proposed by Niu and Ren (1996)

and that of SP5 is nearly the first part of SP2, which means the experiments are repeatable and meet well with each other.

To investigate the damage at strain level, Fig. 16 presents the load-strain curves of SP4 and SP5. As mentioned in the previous section, strain gauges S1-S5 were arranged from top to bottom of the northern steel beam for each specimen so that S1 shows the strain of the upper flange and S5 shows the strain of the lower flange. During the pre-damage test, the strain of steel beam in SP4 varies linearly with respect to the load, while the strain of the lower flange in SP5 tends to enter the yield stage at last few cycles, which could be a supplementary evidence to explain the "S" type phenomenon of the hysteresis curve for SP5.

Table 8 Cumulative hysteretic energy of SP2, SP4, and SP5

Specimen	Loading cycles	E_c (kN·mm)	Percentage
SP2	27	313359	100%
SP4	10	591	0.18%
SP5	20	9750	3.11%

Table 8 shows the cumulative dissipative energy for each specimen after cyclic loading. Furthermore, according to the damage index model proposed by Niu and Ren (1996), the damage index for SP4 and SP5 are 0.16 and 0.32, respectively, as presented in Fig. 17.

3.3 Fire test

Fire test was conducted on intact SP3 specimen, and partially damaged SP4 and SP5 specimens, the results of which have been shown in Table 9. Generally, according to GB/T 9978.1 (2008), 1/20 of the span should be regarded as the maximum allowable deflection for beam and slab. However, the maximum range of installed displacement gage is only 180 mm, which is about 1/30 of the span. Therefore, to compare the fire resistant performance of three specimens, 179 mm (1/30 of the span) is chosen as the limit. Correspondently, the fire endurance in this paper is defined as the heating-up time when the deflection reaches

Table 9 Experimental observations and failure modes of SP3, SP4 and SP5 specimens during fire test

No.	Item	SP3	SP4	SP5
1	Overflow of water at concrete surface cracks	11 mins	12 mins	11 mins
2	Water trace diluting	51 mins	52 mins	55 mins
3	Speeding up of deformation	60 mins	55 mins	45 mins
4	Maximum deflection (179 mm)	101 mins	86 mins	77 mins
5	Total heating time	156 mins	127 mins	113 mins
6	Degree of spalling	severe	moderate	moderate
7	Failure modes observed in all three specimens	Severe deformation Buckling of steel beam Numerous concrete cracks		

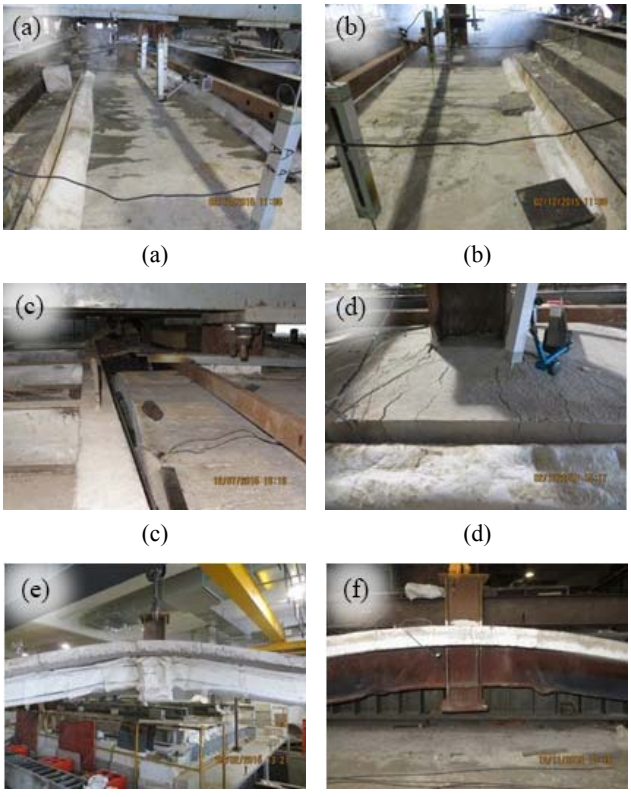

(a) (b)

(c) (d)

(e) (f)

Fig. 18 Experimental observations for SP3 specimen

179 mm. It is indicated from Table 9 that the responses of all three specimens are similar except the extent of spalling occurred in concrete slab.

The experimental observations for SP3 are as follows: Firstly, at about 10 min after heating, overflow of water at cracks on the upper surface of concrete was observed (Fig. 18(a)). The water trace began to dilute at about 50 min after heating (Fig. 18(b)). Meanwhile, vertical deflection at the joint area increased rapidly until reaching maximum deflection (Fig. 18(c)). Finally, specimens failed due to numerous concrete cracks (Fig. 18(d)) and severe deformation followed by buckling at steel beam (Fig.

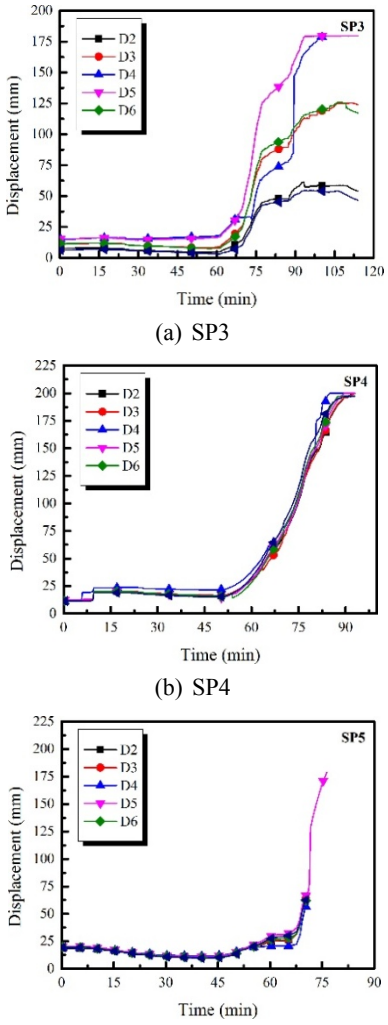

(a) SP3

(b) SP4

(c) SP5

Fig. 19 Displacement-time curves of SP3, SP4 and SP5 specimens under fire test

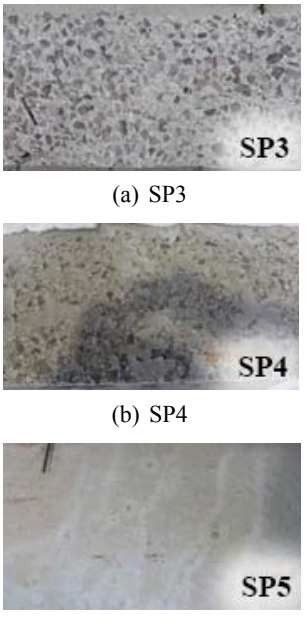

(a) SP3

(b) SP4

(c) SP5

Fig. 20 The extent of spalling concrete slab

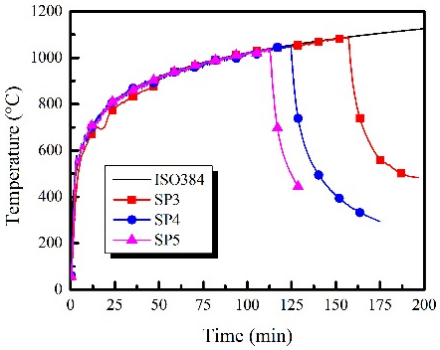

Fig. 21 Temperature of furnace vs. ISO834 standard curve

18(e)). It could be observed after experiment that the lower flanges of the steel beam buckled at the range of 300 mm-700 mm near the steel column (Fig. 18(f)).

From the mechanical point of view, the deformation of the specimens under fire is affected by the thermal expansion and deterioration of material properties at elevated temperatures. At the early stage of heating, contributed by thermal expansion, downward deflection of the joint due to uneven thermal expansion along the cross section was observed. This is because of the temperature gradient over the cross section of the specimen, since the heat is transferred from the lower surface of the specimen to the upper surface and the heat conductivity coefficient of the steel is much larger than that of the concrete. However, the deflection caused by thermal expansion is quite small and ignorable for the whole heating period as shown in Fig. 19. Importantly, the displacement increased from 25 mm to 175 mm lasting only 40 mins, which resulted from the deterioration of material properties after the temperature of the steel member reached 400°C. Although different standards, such as ECCS, EC3, and AS4100, suggest different equations for predicting the steel material properties at elevated temperatures, they all agree that the steel properties (both yield strength and Young's modules) deteriorate significantly over 400°C. Besides, for SP3, after 105 min, the displacement tends to decrease. It is likely to be the result of the catenary action of the steel beam, which makes the beam get tensioned to resist the constant load from jacks.

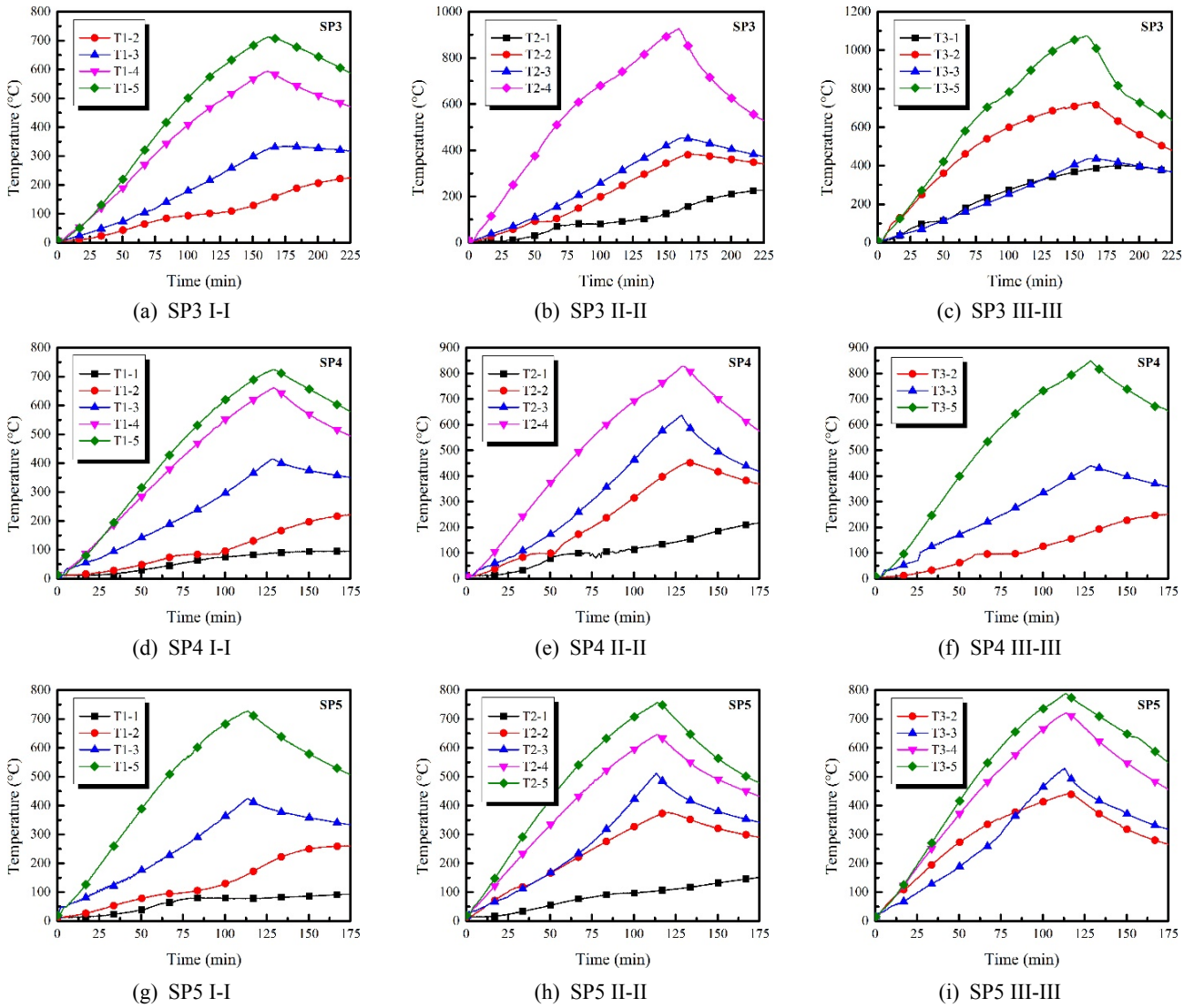

(a) SP3 I-I (b) SP3 II-II (c) SP3 III-III

(d) SP4 I-I (e) SP4 II-II (f) SP4 III-III

(g) SP5 I-I (h) SP5 II-II (i) SP5 III-III

Fig. 22 Temperature distribution along the cross section

According to the test results, the extent of spalling of concrete slab during fire test is related to damage degree of the specimen. As shown in Fig. 20, severe concrete spalling at the lower surface was observed in SP3 specimen while concrete spalling in SP4 and SP5 specimens was moderate. The pre-damage cracks in SP4 and SP5 specimens accelerated the rate of water evaporation in concrete and enhanced the concrete penetrability, which were two crucial factors affecting the spalling. As far as the spalling is concerned, initial damage before fire seems to be beneficial for the steel-concrete composite beam-to-column joints.

4. Analysis and discussion

To better understand the influence of pre-damage deformation on performance of the steel-concrete composite joints at elevated temperatures, all collected data are analyzed and discussed in this section.

4.1 Temperature distribution

The variation of the furnace temperature with time for all fire tests is plotted in Fig. 21 It is seen that the practical furnace temperature curves for all three specimens meet well with ISO834 standard time-temperature curve. As mentioned in the previous sections, fire tests were terminated when the specimens failed to bear the constant load of 152 kN. It is noted that the actual heating-up times for SP3, SP4 and SP5 are 156 mins, 127 mins, and 113 mins, respectively.

As explained in Section 2.3, 15 thermocouples were used evenly at three selected sections for each specimen (SP3, SP4 & SP5) so that each cross-section had five thermocouples as shown in Fig. 9. Due to uncontrollable factors, a few thermocouples recorded invalid data and only valid temperature-time data are shown in Fig. 22. For most of the selected cross-sections of all specimens, the temperature distribution is almost the same, in which the lower flange temperature of steel beam is greater than the web temperature of steel beam. Also, the upper flange temperature of steel beam is greater than the lower surface temperature of concrete slab and this is also higher than the upper surface temperature of concrete slab. Generally, such temperature distributions coincide with the heat transfer law as the heat is transferred from steel beam to concrete slab. However, there is one exception at section III-III of SP3, where the lower surface temperature of concrete slab (T3-2) is higher than the upper flange temperature of steel beam (T3-3). Such exception could be explained by the uncertainty of temperature distribution in the local parts of the furnace.

To discuss the temperature distribution along the length of beam, lower surfaces temperature of the concrete slab at different sections are plotted for each specimen in Fig. 23. Also, variation of temperature at upper flange of the steel beam is plotted in Fig. 24. It is seen that the temperature of section I-I located near the joint area is the lowest among three sections. Given that the specimen was suffering a hogging load under fire, the vertical deflection made section I-I farthest away from the furnace, therefore, the temperature here was lower than other sections.

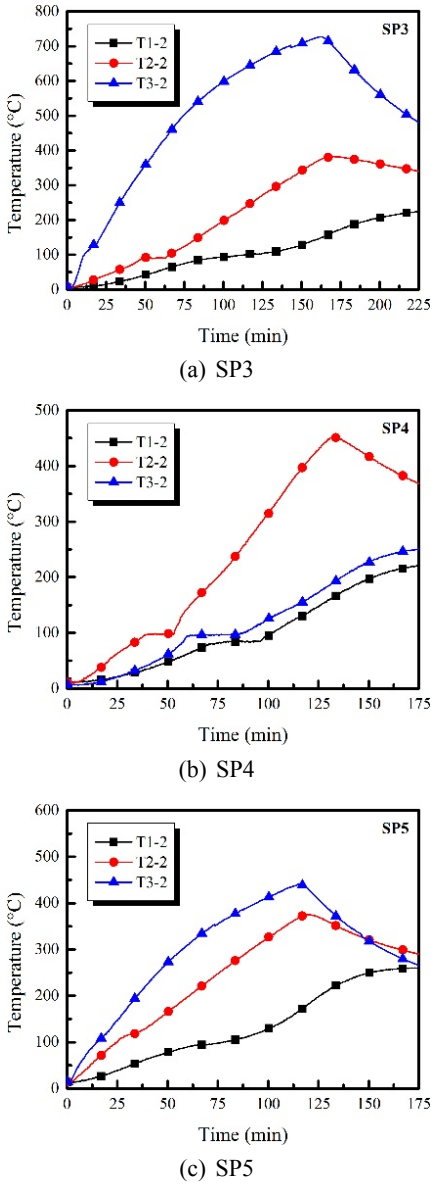

(a) SP3

(b) SP4

(c) SP5

Fig. 23 Temperature distribution along the span in concrete slab

To figure out the influence of damage degree on the fire-resistant performance of steel-concrete composite beam-to-column joint, the average temperatures of the lower surface of concrete slab and the average temperatures of lower flange of steel beam at three different cross sections are calculated and compared together for all three specimens in Fig. 25. For both concrete slabs and steel beams, at the same heating-up time, the temperature of SP5 is always the highest and that of SP3 is always the lowest. However, at the same temperature, SP3 needs more heating-up time than SP4 and SP5 which were affected by pre-damage deformations. In other words, the pre-damage deformation has intensified the heating-up rate so that more severe damage has led to faster heating-up rate. It is also seen that the temperatures of concrete slabs suffer a “lag platform” at the temperature of 100°C. Such a “lag platform” is caused by water evaporation in the concrete slab which starts at the

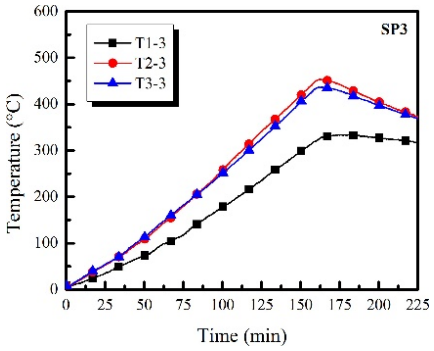

(a) SP3

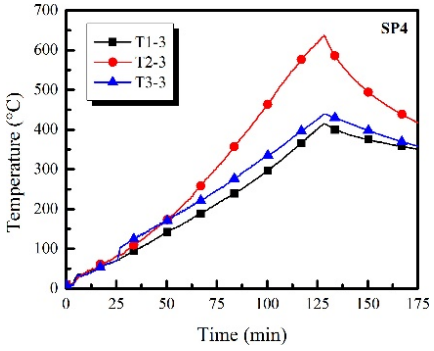

(b) SP4

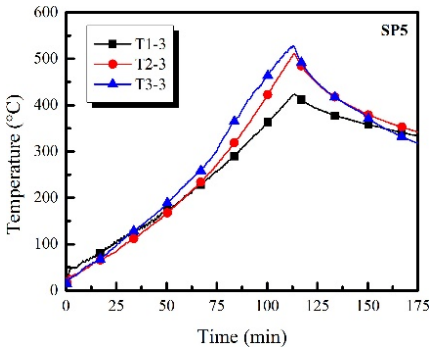

(c) SP5

Fig. 24 Temperature distribution along the span in steel beam

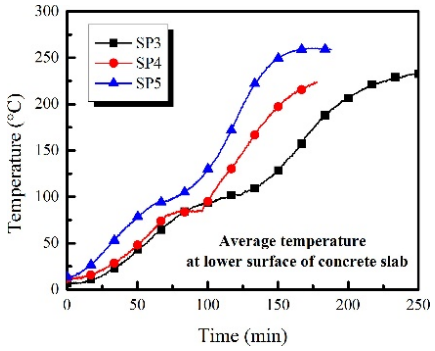

(a) Concrete slab

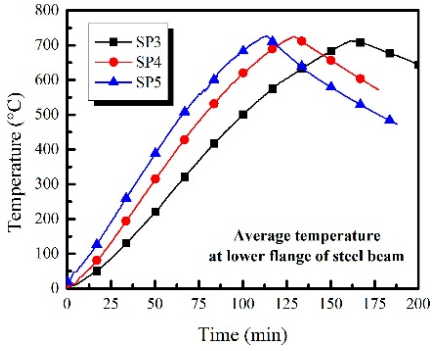

(b) Steel beam

Fig. 25 Temperature at concrete slab and steel beam

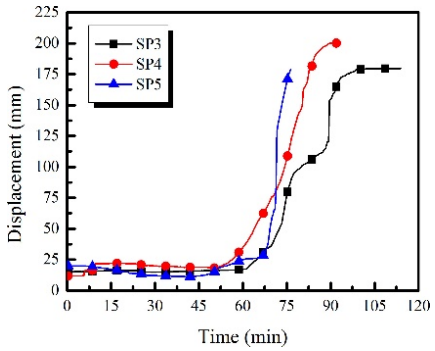

(a) Displacement-time

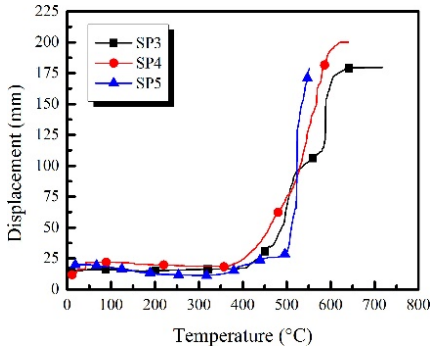

(b) Displacement-temperature

Fig. 26 Displacement at the mid-span of SP3, SP4 and SP5

boiling point of water, i.e., 100°C. Among all three specimens, SP3 exhibits the longest "lag platform" and SP5 presents the shortest one, because pre-damage deformation accelerates the evaporation and enhances the penetrability of the concrete which lead to shorter "lag platform".

4.2 Displacement and temperature

The average value of mid-span displacement for each specimen is depicted in Fig. 26(a). The variation of displacement with time in the first 50mins is negligible for all specimens which means pre-damage deformation shows little influence on the displacement values during early fire. However, to reach displacement values greater than 100 mm, SP5 needs the shortest time while SP3 needs the longest time. In other words, the fire endurance is inversely proportional to the damage degree: more severe damage leads to shorter fire endurance. This is because (i) Pre-damage causes deterioration of mechanical properties of concrete (Note that the applied damage is not severe enough to cause deterioration in steel mechanical properties); and (ii) the pre-damage deformation accelerates the heating-up

Table 10 Comparison of fire duration among SP3, SP4 and SP5 specimens

Specimen	Pre-damage	Damage index	Fire endurance (min)	Relative value
SP3	Intact	0	101	1
SP4	Lower pre-damage deformation	0.16	86	0.85
SP5	Higher pre-damage deformation	0.32	77	0.76

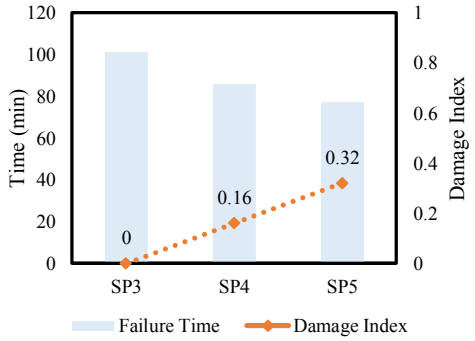

Fig. 27 Fire endurance vs. damage index

rate which means the average temperature of SP5 would be the highest among the tested specimens. This is also demonstrated by the relationship between the displacement of mid-span and the average temperature of the lower flange of steel beam for each specimen as plotted in Fig. 26(b). It is found that when the temperature is lower than 400°C, the curves match well with each other, while after 400°C, the temperature in SP5 increases faster than others. However, the ultimate temperatures for each specimen are similar, which means the fire endurance of the damaged specimens are reduced mainly because of the accelerated heating-up rate instead of deteriorated steel mechanical properties.

4.3 Fire endurance

Fire endurance is the most intuitive index for fire-resistant performance evaluation. The critical failure time of each specimen was defined when the displacement limit of 179 mm was achieved as mentioned in section 3.3. For all three specimens, the fire endurances are listed in Table 10. A quantitative relationship between fire resistance and damage index is also plotted in Fig. 27. As can be seen, failure time decreases as damage degree increases. The failure time of SP4 with lower pre-damage deformation is 15% shorter than that of the intact joint (SP3), and the failure time of SP5 with higher pre-damage deformation is 24% shorter than that of the intact joint (SP3).

The significant damage-induced reduction of fire resistance performance presented above is noticeable and worth consideration in structural design. The result is in accordance with the general conclusion from existing literatures (Alderighi *et al*. 2008, Pucinotti *et al*. 2011a, b) that seismic-induced damage is one of the impact factor for fire resistance performance of structures. For instance, according to their experimental results, the fire duration of pre-damaged interior steel sheeting composite joint was 40 min, while the fire duration of undamaged joint was 60 min. In our research, two different levels of damage were applied to specimens and the result effectively validated and refined the existing conclusion. To better capture the relationship between fire resistance performance and damage degree, more specific experiments and simulations are still needed.

As explained in the previous section, the reduction of fire resistance is mainly due to the cracks in concrete slab which accelerate the heating-up rate of the specimen. Therefore, controlling the heating-up rate is the key measure to promise reliable fire endurance. One possible solution is to enhance the fire protection layer; however, it is not just to make it thicker but also to ensure its effectiveness after cyclic loading. If the damage is severe enough to cause significant deterioration of steel mechanical properties, the fire resistance would be significantly lower.

5. Conclusions

This paper presented the experimental research on fundamental performance of steel-concrete composite beam-to-column joints partially damaged by cyclic loading at elevated temperatures. Monotonic and fire control tests were also conducted. The main conclusions are listed below:

(1) The steel-concrete composite beam-to-column joints exhibited good energy dissipation capacity under cyclic loading. It is seen that the load bearing capacity under monotonic test (316 kN) is slightly higher than that of cyclic test (309 kN), which indicates that the mechanical properties are deteriorated during cyclic loading;
(2) The uneven temperature field in the specimen during heating process led to the reduction of displacement in the first 50 mins of heating-up process, since the heat conductivity coefficient of steel material is much larger than that of concrete. This part of deformation is benefit for the joint safety but is ignorable compared to the property-deterioration-caused deformation above 400°C;
(3) Different damage degrees of the joints caused different fire-resistant performance. It is evident from the experimental results that the more severe initial damage leads to more cracks in the joint and also shorter “lag platform”. It also mitigates the concrete spalling. Besides, more severe damage leads to the faster temperature rise and shorter fire endurance;
(4) To improve the fire endurance of the joint under post-earthquake fire, it is important to control the heating-up rate of the joint, since the reduction in fire endurance is mainly induced by the acceleration of heating-up rate. One possible solution might be enhancing the seismic performance of the fire protection layer so that it could still be effective under post-earthquake fire.

Acknowledgments

The research work presented in this paper was supported by the National Natural Science Foundation of China (NSFC) through Research Fund for International Young Scientists (Project No. 5135011234) awarded to the third author.

References

Alderighi, E., Bursi, O., Franssen, J.M., Lennon, T., Mallardo, R. and Pucinotti, R. (2008), "Fire Performance of undamaged and pre-damaged welded steel-concrete composite beam-to-column joints with concrete filled tubes", *Proceedings of the 14th World Conference on Earthquake Engineering*, Beijing, China.

Amadio, C., Bedon, C., Fasan, M. and Pecce, M.R. (2017), "Refined numerical modelling for the structural assessment of steel-concrete composite beam-to-column joints under seismic loads", *Eng. Struct.*, **138**, 394-409.

Azhari, F., Heidarpour, A. and Zhao, X.L. (2018), "On the use of Bernstain-Bézier functions for modelling the post-fire stress-strain relationship of ultra-high strength steel (Grade 1200)", *Eng. Struct.*, **175**, 605-616.

Dubina, D., Ciutina, A.L. and Stratan, A. (2002), "Cyclic tests on bolted steel and composite double-sided beam-to-column joints", *Steel Compos. Struct., Int. J.*, **2**(2), 147-160.

FEMA-461 (2007), Interim testing protocols for determining the seismic performance characteristics of structural and nonstructural components; Applied Technology Council, CA, USA.

GB/T 9978.1 (2008), Fire-resistance tests - Elements of building construction - Part I: General requirements; Standardization administration of the PRC, Beijing, China.

Jiang, S.C., Guo, X.N., Xiong, Z., Cai, Y.F. and Zhu, S.J. (2017), Experimental studies on behavior of tubular T-joints reinforced with grouted sleeve, *Steel Compos. Struct., Int. J.*, **23**(5), 585-596.

Kato, B., Tanaka, A. and Yamanouchi, H. (1980), "A field work investigation of steel building damage due to the 1978 Miyagiken-oki earthquake", *Proceedings of the Seventh World Conference on Earthquake Engineering*, Istanbul, Turkey, July.

Li, F., Zhao, Q.L., Chen, H.S. and Xu, L.X. (2017), "Experimental investigation of novel pre-tightened teeth connection technique for composite tube", *Steel Compos. Struct., Int. J.*, **23**(2), 161-172.

Liew, J.Y.R., Teo, T.H. and Shanmugam, N.E. (2004), "Composite joints subject to reversal of loading - Part 1: experimental study", *J Constr. Steel Res.*, **60**(2), 221-246.

Ma, H.W., Jiang, W.S. and Cho, C.D. (2011), "Experimental study on two types of new beam-to-column connections", *Steel Compos. Struct., Int. J.*, **11**(4), 291-305.

Mirmomeni, M., Heidarpour, A., Zhao, X.L. and Packer, J.A. (2017), "Effect of elevated temperature on the mechanical properties of high-strain-rate-induced partially damaged concrete and CFSTs", *Int. J. Impact Eng..*, **110**, 346-358.

Niu, D.T. and Ren, L.J. (1996), "A modified seismic damage model with double variables for reinforced concrete structures", *Earthq. Eng. Eng. Vib.* (*Chinese*), **164**, 44-54.

Pecce, M. and Rossi, F. (2015), "The experimental behavior and simple modeling of joints in composite MRFs", *Eng. Struct.*, **105**, 249-263.

Pucinotti, R., Bursi, O.S. and Demonceau, J.F. (2011a), "Post-earthquake fire and seismic performance of welded steel–concrete composite beam-to-column joints", *J. Constr. Steel Res.*, **67**(9), 1358-1375.

Pucinotti, R., Bursi, O.S. and Franssen, J.M. (2011b), "Seismic-induced fire resistance of composite welded beam-to-column joints with concrete-filled tubes", *Fire Safety J.*, **46**(6), 335-347.

Santiago, A., da Silva, S.L, Vaz, G., Vila, R.P. and Lopes, A.G. (2008), "Experimental investigation of the behavior of a steel sub-frame under a natural fire", *Steel Compos. Struct., Int. J.*, **8**(3), 243-264.

Sevim, B. (2017), "Structural response of rectangular composite columns under vertical and lateral loads", *Steel Compos. Struct., Int. J.*, **25**(3), 287-298.

Sinaie, S., Heidarpour, A. and Zhao, X.L. (2014), "Stress-strain-temperature relation for cyclically-damaged structural mild steel", *Eng. Struct.*, **77**, 84-94.

Song, Q.Y., Heidarpour, A. and Zhao, X.L. (2017), "Post-earthquake fire performance of flange-welded/web-bolted steel I-beam to hollow column tubular connections", *Thin-Wall. Struct.*, **116**, 113-123.

Tremblay, R., Bruneau, M., Nakashima, N., Prion, H.G.L., Filiatrault, A. and DeVall, R. (1996), "Seismic design of steel buildings: Lessons from the 1995 Hyogo-ken Nanbu earthquake", *Can. J. Civ. Eng.*, **23**(3), 727-756.

Valente, I.B. and Cruz, P.J.S. (2010), "Experimental analysis on steel and lightweight concrete composite beams", *Steel Compos. Struct., Int. J.*, **10**(2), 169-185.

Xiao, X.F., Zeng, L., Cui, Z.K., Jin, S.Q. and Chen, Y.G. (2017), "Experimental and analytical performance evaluation of steel beam to concrete-encased composite column with unsymmetrical steel section joints", *Steel Compos. Struct., Int. J.*, **23**(1), 17-29.

Zhu, X.H., Li, B.Y., Gan, D., Liu, J.P. and Chen, Y.F. (2017), "Connections between RC beam and square tubed-RC column under axial compression: Experiments", *Steel Compos. Struct., Int. J.*, **23**(4), 453-464.

BU